Waveguiding properties of short linear chains of nonspherical metal nanoparticles

Ilia L. Rasskazov,[1,2,*] Sergei V. Karpov,[1,2,3] and Vadim A. Markel[4]

[1]*L. V. Kirensky Institute of Physics, Krasnoyarsk 660036, Russia*
[2]*Laboratory for Nonlinear Optics and Spectroscopy and Department of Photonics and Laser Technologies, Siberian Federal University, Krasnoyarsk 660041, Russia*
[3]*Siberian State Aerospace University, Krasnoyarsk 660014, Russia*
[4]*Departments of Radiology and Bioengineering and the Graduate Group in Applied Mathematics and Computational Science, University of Pennsylvania, Philadelphia, Pennsylvania 19104, USA*
**Corresponding author: il.rasskazov@gmail.com*

Received September 11, 2014; revised October 13, 2014; accepted October 13, 2014;
posted October 14, 2014 (Doc. ID 222807); published November 7, 2014

We study numerically the discrete dispersion relations and waveguiding properties of relatively short linear chains of spherical and spheroidal silver nanoparticles. Simulations are based on the Drude model for the dielectric permittivity of metal and on the dipole approximation for the electromagnetic interaction of particles. We also simulate the dynamics of femtosecond optical pulse propagation along such chains. In the case that we consider (10 particles per chain), reflections from the chain terminals play a significant detrimental role. We show that dissipative traps can be used to reduce the effects of reflections. We also show that chains composed of oblate spheroids with sufficiently small aspect ratio (nanodisks) have better waveguiding properties when compared to chains made of particles with other spheroidal shapes. This includes a slower rate of decay, larger group velocity, and larger bandwidth.

OCIS codes: (240.5420) Polaritons; (240.6680) Surface plasmons; (250.5530) Pulse propagation and temporal solitons; (250.5403) Plasmonics.
http://dx.doi.org/10.1364/JOSAB.31.002981

1. INTRODUCTION

The waveguiding properties of chains of closely spaced metallic nanoparticles (plasmonic chains) have been extensively discussed in the physics and engineering literature over the past decade or so [1–11]. Such systems can be useful for transmission of modulated optical signals with a high degree of spatial confinement. Localization of electromagnetic fields is an important consideration in applications related to the development of nanoscale optical elements. For instance, the subwavelength spatial localization of optical excitations in plasmonic chains can be expected to minimize parasitic interactions between different elements in an optical circuit. Alternative designs of nanoscale waveguides have also been considered in the literature, including nanowires [12,13] and nanogrooves on a flat surface [13,14], as well as strips, ridges, and other similar structures [15]. It is difficult to tell at present which design is more promising. However, plasmonic chains are characterized by the exceptional tunability of their physical properties.

Optical signals propagate in plasmonic chains in the form of surface plasmon polaritons (SPPs), which are collective excitations of the conductivity electrons and the electromagnetic field. SPPs can be characterized by a dispersion relation, and from the latter one can determine the group and phase velocities. Dispersion relations for relatively long plasmonic chains consisting of $N \approx 10^3$ particles have been studied extensively for both spherical [3,5,16–24] and nonspherical particle shapes [1,4,17]. In particular, it was shown that SPP group velocities in chains of spherical particles are much smaller than the speed of light, c. As a consequence, the bandwidth of such waveguides is severely limited. This problem can be rectified by using nonspherical particles [4,25]. In plasmonic chains made of spheroidal particles with sufficiently small aspect ratio, the group velocities can be of the order of c, and the spectral interval where the dispersion relation is close to linear (the bandwidth) can be sufficiently large to allow for propagation of well-shaped wave packets [4]. However, ohmic losses strongly affect SPPs in long chains. There exist designs wherein transmission of wave packets through long chains is possible with virtually no decay of the amplitude [26,27], but these designs require large energy input at the first particle of the chain, which can cause significant heating.

Due to this and other reasons, relatively short chains are of interest. In plasmonic chains consisting of $N \lesssim 20$ particles, ohmic losses are negligible, which is a valuable property for practical applications. Also, short chains can be required for miniaturization purposes. Dispersion relations in relatively short plasmonic chains of spherical particles have been considered in the literature [18,20,28]. However, short plasmonic chains also have disadvantages, in particular, the parasitic effect of SPP reflections from the chain terminals. Propagation of SPP wave packets in short chains, particularly in the case in which the chains are made of nonspherical particles, has received little attention so far.

In this paper, we study numerically the waveguiding properties of short chains of both spherical and spheroidal particles and introduce the idea of a dissipative trap, which

can suppress SPP reflection from the chain terminals. We consider perfectly ordered chains and note that slight position disorder is not expected to have a dramatic effect [29–31].

The paper is organized as follows. In Section 2, we formulate the theoretical model, which is used in the simulations. Section 3 summarizes the physical parameters and simulation methods that are used in the remainder of this paper. Section 4 presents the numerical results for dispersion relations and group velocities. In Section 5 we present real-time numerical simulations of femtosecond pulse propagation through short chains. Section 6 contains a summary of obtained results.

2. THEORY

In this work, we write the equations that describe the electromagnetic interaction of particles in the frequency domain. Correspondingly, all physical quantities that enter these equations are functions of the frequency ω. However, description of transient processes requires transformation of the frequency-domain solutions into the time domain. For any frequency-domain function $f(\omega)$, we write

$$f(t) = \int f(\omega) \exp(-i\omega t) \frac{d\omega}{2\pi}. \quad (1)$$

For economy of notations, we have used the same symbol for the time- and frequency-domain functions, and the same approach is used in the rest of the paper. This should not cause confusion because the domain in which a function is considered should always be clear from the context.

A. Electromagnetic Interaction Model

Consider a linear chain consisting of N particles of spherical or spheroidal shape (see Fig. 1). The centers of spheroids are located along the Z axis at the points $z_n = nh$, where h is the chain period. We assume that the spheroids are electrically small and work in the dipole approximation, according to which each spheroid is characterized by the dipole moment $d_n(\omega)$ and

$$\mathbf{d}_n(\omega) = \alpha(\omega)\mathbf{E}_n(\omega) = \alpha(\omega)[\mathbf{E}_n^{(\mathrm{inc})}(\omega) + \mathbf{E}_n^{(\mathrm{scatt})}(\omega)]. \quad (2)$$

Here, $\mathbf{E}_n(\omega)$ is the electric field *external* to the nth dipole, which is given by a superposition of the field *incident* from external sources, $\mathbf{E}_n^{(\mathrm{inc})}(\omega)$, and the field *scattered* by all other dipoles in the chain, $\mathbf{E}_n^{(\mathrm{scatt})}(\omega)$, and $\alpha(\omega)$ is the polarizability tensor. The relevant mathematical details of the dipole approximation are given elsewhere [4,29,32].

A simplification of Eq. (2) can be obtained if we account for certain special symmetries. In this paper we consider linear chains composed of spheroids, which are all similarly oriented in space so that one of the principal axes of any spheroid is parallel to the chain (see Fig. 1). In this case, SPPs that are polarized transversely and parallelly to the chain are electromagnetically decoupled. Correspondingly, the vector Eq. (2) can be factored into three independent scalar equations. Each scalar subsystem contains the appropriate principal element of the polarizability tensor $\alpha(\omega)$. In what follows, we consider differently polarized SPPs separately and characterize each case by a set of complex scalar amplitudes $d_n(\omega)$. The notation $\alpha(\omega)$ will refer to the appropriate principal element of the polarizability tensor.

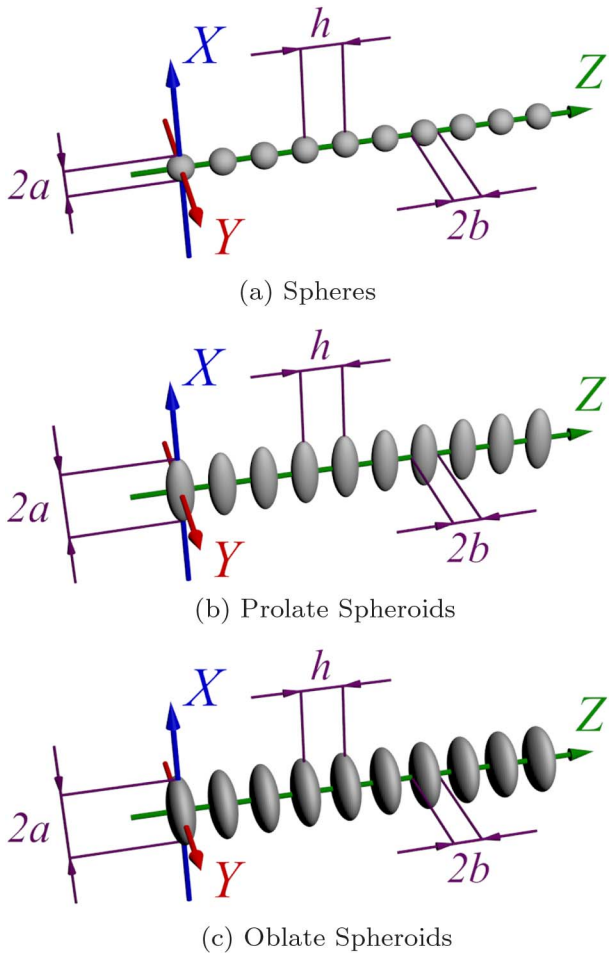

Fig. 1. Schematic view of chains used in the simulations.

B. Discrete Dispersion Relations

According to the standard approach, we determine the dispersion relation by seeking nontrivial solutions to the homogeneous coupled-dipole equation, that is, for $\mathbf{E}_n^{(\mathrm{inc})}(\omega) = 0$. In the absence of external field and for a fixed polarization of SPPs, Eq. (2) assumes the form

$$d_n(\omega) = \alpha(\omega) \sum_{m=1}^{N} (1 - \delta_{nm}) G_{nm}(\omega) d_m(\omega). \quad (3)$$

Here, $G_{nm}(\omega)$ is the diagonal element of the Green's tensor for the electric field in free space; the mathematical form of $G_{nm}(\omega)$ is given, for example, in [4,29,32]. The homogeneous system of N Eq. (3) has a nontrivial solution if and only if

$$\det[M(\omega)] = 0, \quad (4)$$

where the matrix elements of $M(\omega)$ are given by the expression

$$M_{nm}(\omega) = \delta_{nm} - (1 - \delta_{nm})\alpha(\omega)G_{nm}(\omega). \quad (5)$$

The complex roots Ω_k of Eq. (4) are known as the natural frequencies [33,34]. We note that if Ω_k is a natural frequency, then $-\Omega_k^*$ is also a natural frequency, assuming that we have used correct analytical expressions for $\alpha(\omega)$ and $G_{nm}(\omega)$. Further, it can be expected on physical grounds that, in systems

without gain, all natural frequencies satisfy $\mathrm{Re}(\Omega_k)\,\mathrm{Im}(\Omega_k) < 0$ [equivalently, $\mathrm{Im}(\Omega_k^2) < 0$]. In other words, oscillations with positive frequencies are decaying with time [17,18,29].

In the general case, Eq. (4) is a transcendental equation, which has an infinite number of roots even if the number of particles is finite. If one uses the analytical Drude formula for the metal permittivity (as is done here) and the quasi-static approximation for the Green's function, then Eq. (4) becomes an algebraic equation with exactly $2N$ roots, taking into account the degeneracy noted above. In this paper, the quasi-static approximation is not used. Therefore, the number of roots is infinite and we use a numerical root-searching procedure (described below) to find the first N natural frequencies with $\mathrm{Re}(\Omega_k) > 0$ and the smallest values of $-\mathrm{Im}(\Omega_k) > 0$. We have found empirically that, for the physical system considered in this paper, the natural frequencies outside of this finite set have very large values of $-\mathrm{Im}(\Omega_k)$ and the corresponding oscillation modes are characterized by very short lifetimes. Such modes do not contribute noticeably to any physical observables.

The above procedure defines a set of complex natural frequencies Ω_k, $k = 1, \ldots, N$. To find the dispersion relation, we use the approach of [18]. Namely, a *real* wave number q_k corresponding to the natural frequency Ω_k is defined by the expression

$$q_k = \frac{(N-2)m_k + 1}{N(N-1)}\frac{\pi}{h}, \tag{6}$$

where m_k is the kth mode index. To compute m_k, we first need to determine the eigenvectors (the polarization modes) that correspond to each natural frequency. The procedure for computing m_k is explained next.

Consider the eigenvalues $\lambda_n(\omega)$ and eigenvectors $|x_n(\omega)\rangle$ of $M(\omega)$, which satisfy the frequency-parameterized eigenproblem

$$M(\omega)|x_n(\omega)\rangle = \lambda_n(\omega)|x_n(\omega)\rangle. \tag{7}$$

Since the size of $M(\omega)$ is N, there exist at most N linearly independent eigenvectors $|x_n(\omega)\rangle$. In practice, this number is equal to N because $M(\omega)$ is not defective. We now consider these quantities at $\omega = \Omega_k$. Since $\det[M(\Omega_k)] = 0$, at least one of the eigenvalues $\lambda_n(\Omega_k)$ is zero. It can be expected that the zero eigenvalues are not degenerate, and we have confirmed this fact numerically. If we arrange the eigenvalues in the ascending order, then

$$0 = \lambda_1(\Omega_k) < \lambda_2(\Omega_k) \le \ldots \le \lambda_N(\Omega_k).$$

The eigenvectors that correspond to the zero eigenvalues, $|g_k\rangle \equiv |x_1(\Omega_k)\rangle$, are the *waveguiding modes*. To find the mode index m_k, we determine the number of times the expression $\mathrm{Re}\langle i|g_k\rangle$, viewed as a function of i, changes sign. Here $i = 1, \ldots, N$ labels the eigenvector components. The mode index m_k is defined as this number of sign changes plus 1.

Using the above prescription, we can compute the wave number q_k for each natural frequency Ω_k. Ordered pairs (q_k, Ω_k) define the discrete dispersion relation of the chain. We note that the approach described here is the discrete version of the complex-ω approach as defined in [35]. According to this approach, a complex-valued frequency is found for each purely real wave vector q.

3. SIMULATION PARAMETERS AND METHODS

In the simulations, we consider plasmonic chains consisting of oblate and prolate spheroids (including the special case of spheres) with different aspect ratios $\xi = b/a$, where b and a are the shorter and longer semi-axes. In the case of prolate spheroids, their axes of symmetry (the longer axes) are aligned perpendicular to the chain (along the X axis as shown in Fig. 1). In the case of oblate spheroids, the axes of symmetry (the shorter axes) are aligned parallel to the chain (along the Z axis). The shorter semi-axes of all spheroids (radius in the case of spheres) are fixed at $b = 8$ nm. The longer semi-axes (always oriented perpendicularly to the chain) vary from $a = 8$ nm (in the case of spheres) to $a = 20$ nm. The latter case corresponds to the spheroid aspect ratio $\xi = b/a = 0.4$. The center-to-center separation of nearest spheroids in a chain is in most cases fixed at $h = 24$ nm. However, in some of the figures, h varies from 24 to 32 nm to illustrate the effect of interaction strength on the dispersion relation. The number of particles in the chains is set in most cases to $N = 10$. However, when we consider below a dissipative trap, we work, essentially, with a $N = 60$ chain but assume that the signal is read out at the site of the 10th dipole. The rest of the chain (the tail) serves in this case as a trap that suppresses the effect of parasitic reflections.

A special comment on SPP polarization is necessary. In all cases that we consider, the longer axes of the spheroids are perpendicular to the chain as shown in Fig. 1. It can be seen that, in the case of oblate spheroids, the chains are cylindrically symmetric. As a result, all SPP polarizations that are orthogonal to the chain are equivalent. However, this is not so for the case of prolate spheroids, wherein the cylindrical symmetry of the chain is absent. For prolate spheroids, we will only consider the transverse SPP polarization that is aligned with the longer axes of spheroids. We will refer to this polarization that is transverse to the chain as T polarization and to the polarization that is parallel to the chain as L polarization.

Although we use the retarded Green's functions $G_{nm}(\omega)$ to describe the electromagnetic interaction of particles in a chain, the particles themselves were assumed to be sufficiently small for the quasi-static approximation to be applicable for the purpose of computing the polarizability α. To this end, we use the standard electrostatic result for spheroids [34] with the account of first nonvanishing radiative correction [36,37]. Relevant formulas are given, for example, in [38]. These formulas contain the permittivity of particles $\epsilon(\omega)$. For the latter, we have used the Drude formula

$$\epsilon(\omega) = \epsilon_0 - \frac{\omega_p^2}{\omega(\omega + i\gamma)}, \tag{8}$$

where γ is the relaxation constant, ω_p is the plasma frequency, and $\epsilon_0 - 1$ is the contribution to the permittivity due to the interband transitions. In the simulations, we have used the experimental parameters of silver, viz., $\gamma/\omega_p = 1/526.3$ and $\epsilon_0 = 5$.

To find the natural frequencies Ω_k, we use the following method. First, we compute $|\det[M(\omega)]|$ for the argument ω sampled on the rectangular grid in the complex plane, that

is, for $\omega = \omega_{nm} = (n + im)\Delta$, where $i = \sqrt{-1}$, Δ is the lattice step, and n, m are integers. This task is computationally feasible because the matrix M is of sufficiently small size. We say that ω_{nm} is a local minimum for a given grid if $|\det[M(\omega_{nm})]|$ is smaller than $|\det[M(\omega_{n'm'})]|$ in the eight neighboring points $(n'm')$. We then select the first N local minima Ω_k located in the right half-plane with the smallest values of $-\mathrm{Im}(\Omega_k)$. Next we recompute $|\det[M(\omega)]|$ on a finer grid around each local minimum until the condition $\det[M(\Omega_k)] = 0$ is satisfied with a predetermined precision.

Finally, in some of the figures, we show continuous dispersion curves for infinite chains. These curves were computed by the method described in Section 3.A of Ref. [4]. We note that in this method a purely real dispersion relation is sought for an ideal (lossless) metal, that is, for the case in which Drude relaxation constant γ is set to zero in Eq. (8). It was pointed out recently [35] that this approach is not always accurate in the presence of realistic losses. However, for the parameters used, we have obtained reasonable qualitative agreement between the discrete dispersion relations of a finite chain with realistic losses and the continuous dispersion relations of infinite chains made of lossless metal. We believe that the numerical discrepancies that *are* present in the data can be explained for the most part by the effects of finite length rather than by the effects of losses.

4. RESULTS: DISPERSION RELATIONS

The first task one faces in computing the discrete dispersion relations is determination of the mode indices m_k. Figure 2 illustrates how these quantities were determined for a chain of spherical particles (see figure caption for details). Analogous plots for other parameters of the chain and other polarizations of SPPs look very similar and are not shown here.

We note that the dashed lines connecting the centered symbols in Fig. 2 are shown only to guide the eye; the intermediate values of the displayed functions have no physical meaning. However, the discrete data points shown in the figure can be viewed, approximately, as samples of a smooth function $\cos(qz + \phi)$, where ϕ is a phase shift, taken at the sampling points $z_i = hi$. This identification is obviously not very accurate due to the finite length of the chains (hence, the effects of scattering and reflection from the chain terminals). However, in the numerical example considered here we can find such values q that, sufficiently far from the chain ends, the discrete points sample the smooth function with reasonable precision. The above observation justifies the use of the mode index to determine the wave numbers q_k of the waveguiding modes. The procedure becomes increasingly precise as the number of particles in the chain is increased.

In Fig. 3, we show the dispersion relations and the group velocities, defined here as $v_g = \partial \mathrm{Re}(\Omega)/\partial q$ [39], for chains made of spherical particles ($a = b = 8$ nm) with different values of the center-to-center distance h. We also plot in this figure the continuous dispersion curves of infinite chains, which were computed as described in [4]. It can be seen that the discrete and continuous dispersion relations are in qualitative agreement, with the most pronounced differences visible near the light line. This is not surprising because close to the light line SPPs exist due to the interaction (constructive interference) of a large number of particles. In the relatively short chains considered here, this effect is absent. Overall, the

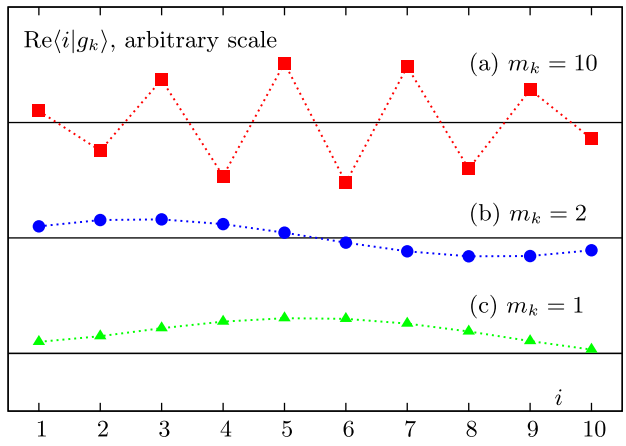

Fig. 2. Illustration of the waveguiding modes for different natural frequencies Ω_k and different corresponding mode indices m_k. Eigenvector components $\mathrm{Re}\langle i|g_k\rangle$ are plotted as functions of i. Computations were performed for a chain of $N = 10$ spherical particles of radius 8 nm, center-to-center separation of $h = 32$ nm, and L polarization of SPPs. The modes shown correspond to the natural frequencies with the real parts (a) $\mathrm{Re}(\Omega_k) \approx 0.3827\omega_p$, (b) $\mathrm{Re}(\Omega_k) \approx 0.3724\omega_p$, and (c) $\mathrm{Re}(\Omega_k) \approx 0.3710\omega_p$. Solid horizontal lines indicate the positions of zero of the vertical axis for each mode. Dashed lines are drawn to guide the eye.

good qualitative agreement between the discrete and continuous dispersion curves for chains consisting of only 10 particles, which we have confirmed numerically, could not be expected *a priori*.

Imaginary parts of the natural frequencies for a chain of spherical particles are shown in Fig. 4. The quantities $-\mathrm{Im}(\Omega_k)$ determine the rate of decay of the waveguiding

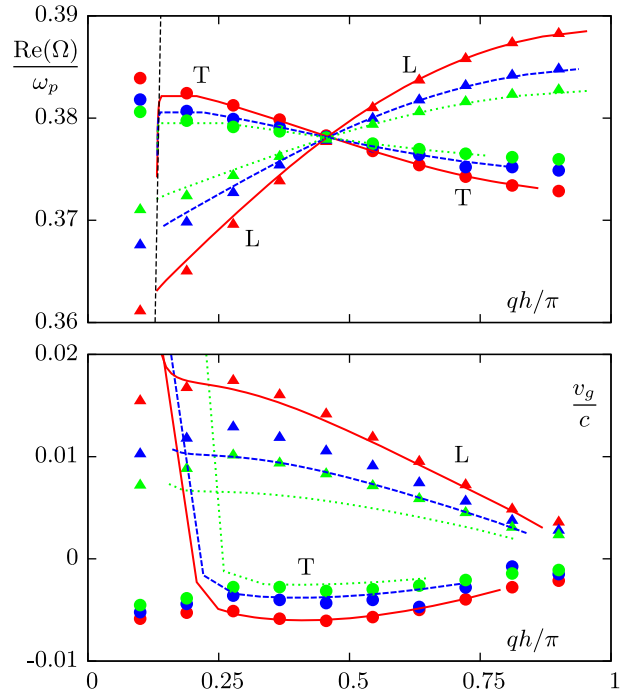

Fig. 3. Dispersion relations (top) and group velocities (bottom) for a chain of $N = 10$ spherical particles 8 nm in radius for T (circles) and L (triangles) SPP polarization. Centered symbols represent the discrete dispersion relations of finite chains. Lines show the respective results in infinite chains. The center-to-center distance h is 24 nm (red color, solid lines), 28 nm (blue color, long dash), and 32 nm (green color, short dash).

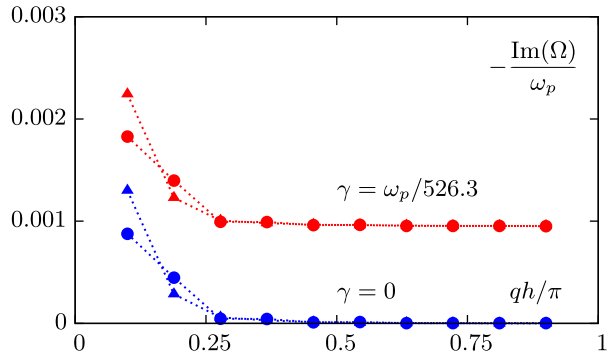

Fig. 4. Imaginary parts of the natural frequencies for a chain whose dispersion relation is illustrated in Fig. 3 (the one with $h = 24$ nm) versus the wave number q for T (circles) and L (triangles) SPP polarization. Calculations were performed for different values of the Drude relaxation constant (realistic and lossless metal), as labeled.

modes due to both ohmic and radiative losses. The contribution of purely radiative losses can be approximately determined by computing $-\mathrm{Im}(\Omega_k)$ for an ideal (lossless) metal, that is, for the case in which $\gamma = 0$. These data points are also shown in Fig. 4. It can be seen that radiative losses dominate for the waveguiding modes with relatively small wave numbers, whose dispersion points are close to the light line. These modes are strongly affected by the loss of translational invariance of the chain and, as a result, are "leaky." In contrast, the modes with relatively large wave numbers are almost free from radiative losses. These modes are quantitatively similar to the modes of infinite chains. By comparing the data for $\gamma = 0$ and $\gamma = \omega_p/526.3$, we can conclude that ohmic losses dominate for all modes with the mode indices $m_k > 2$.

The data shown in Fig. 3 are in agreement with the previously reported observation [4] that the SPP group velocities in chains of spherical particles are very small compared to c, which is not conductive for waveguiding applications. It was also shown in [4] that the SPP group velocities can be substantially increased in chains of nonspherical particles whose longer semi-axes a are oriented perpendicularly to the chain, while the shorter semi-axes b are parallel to the chain, assuming that we keep the ratio h/b fixed, where h is the center-to-center separation of spheroids. This is the physical situation that we consider next. Namely, we now compute the discrete dispersion relations and group velocities for chains of prolate and oblate spheroids with varying aspect ratios $\xi = b/a$. In these simulations, the center-to-center separation is fixed to $h = 24$ nm, and the shorter spheroid semi-axes (always oriented parallel to the chain) are fixed at $b = 8$ nm. We therefore have $h/b = 3$ in all cases considered.

In Fig. 5 we show the dispersion relations and group velocities for chains of prolate and oblate spheroids. It can be seen that the SPP group velocities in the case of spheroids with $\xi = 0.4$ are significantly larger than in the case of spheres. For example, for oblate spheroids we obtain $|v_g| \approx 0.10c$ for L polarization and $|v_g| \approx 0.09c$ for T polarization. This is an order of magnitude larger than the corresponding group velocity values in chains of spherical particles, yet still an order of magnitude smaller than c. Thus, we do not achieve the same high group velocities (of the order of c or even larger) as in [4]. For this, even smaller aspect ratios are required. However, further reduction of the aspect ratio results in increased radiative losses. This effect is not present in infinite chains where radiative losses are absent in principle, but in the short chains

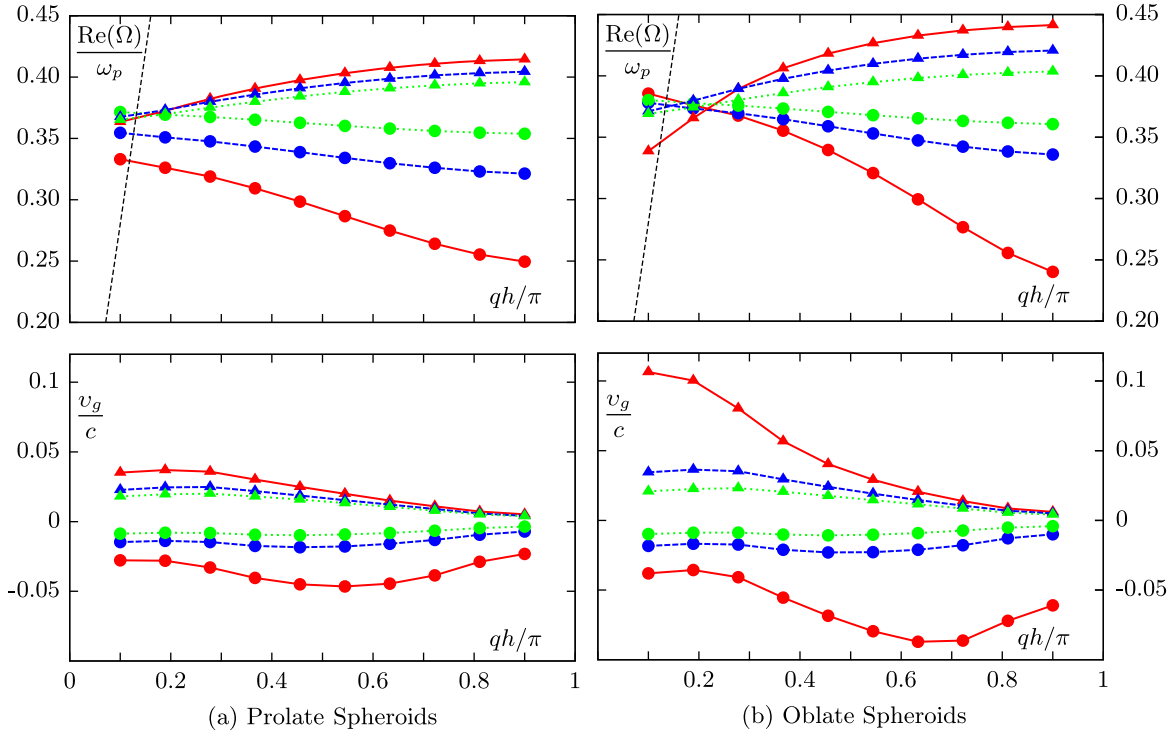

Fig. 5. Dispersion relations (top) and group velocities (bottom) for chains consisting of $N = 10$ prolate (left) and oblate (right) spheroids for T (circles) and L (triangles) SPP polarization. Calculations were performed for fixed center-to-center distance $h = 24$ nm, fixed small semi-axis $b = 8$ nm, and varying long semi-axis a, which corresponds to the following aspect ratios: $\xi = b/a$:0.4 (red, solid lines), 0.6 (blue, long dash), and 0.8 (green, short dash). The black dotted line corresponds to the light line.

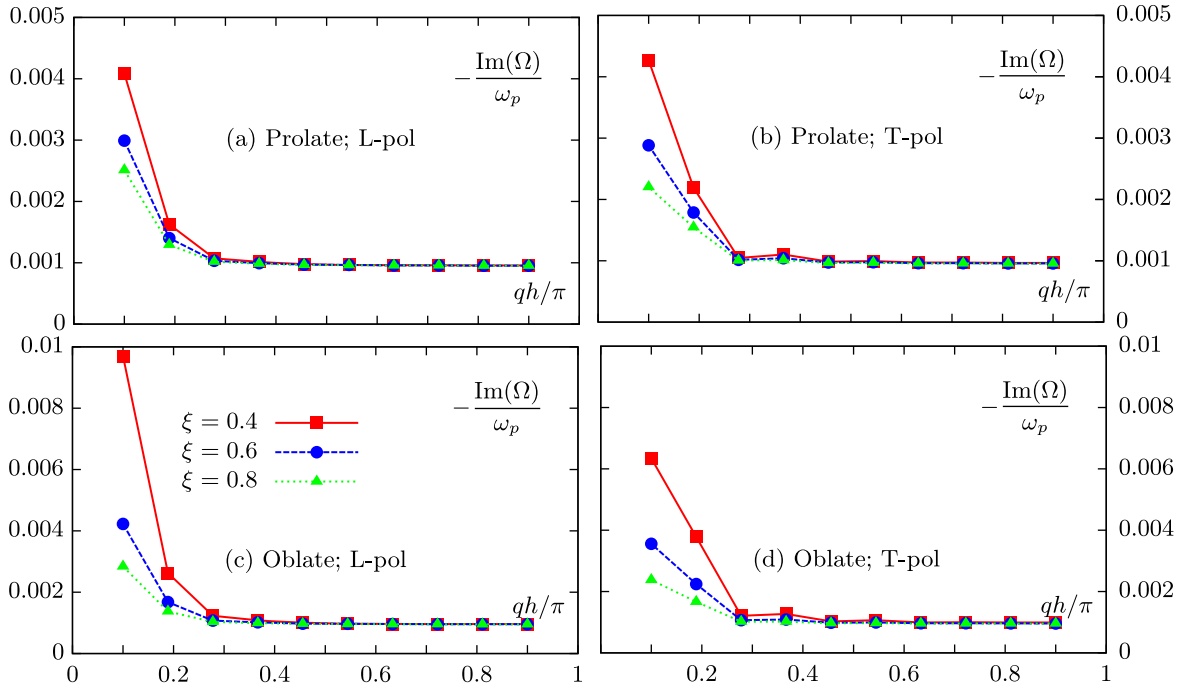

Fig. 6. Imaginary parts of the natural frequencies for chains of $N = 10$ prolate (top) and oblate (bottom) spheroids for L polarization (left) and T polarization (right). Aspect ratio $\xi = b/a$ as labeled. The shorter semi-axis is fixed at $b = 8$ nm, and the center-to-center particle separation is $h = 24$ nm.

considered here, it is significant. The dependence of radiative losses (imaginary parts of the natural frequencies) on the aspect ratio is illustrated in Fig. 6. It can be seen that the few waveguiding modes that are most affected by the finite length of the chain (typically, the three modes with the smallest wave numbers) have radiative decay rates that are strongly affected by the aspect ratio. Already at $\xi = 0.4$, these losses are significant, and further reduction of ξ appears, therefore, to be impractical in the case of short chains. We further observe that the decay rates are typically smaller in the case of oblate spheroids.

We conclude this section by noting that reducing the aspect ratio of spheroids in finite chains results in larger SPP group velocities but also in larger radiative losses. Based on the analysis of dispersion relations (Figs. 3 and 5) and radiative decay rates (Figs. 4 and 6), it can be stated that short linear chains of oblate spheroids are more suitable for transmission of optical pulses than chains of spheres or prolate spheroids. Moreover, the aspect ratio of $\xi = 0.4$ appears to be an acceptable compromise between the need to increase the SPP group velocity and to reduce radiative losses.

5. RESULTS: TRANSIENT PROCESSES

To simulate wave packet propagation in the time domain, we use the approach described in Ref. [4]. We assume that the first particle in the chain is illuminated by a Gaussian pulse with center frequency ω_0 and spectral width $\Delta\omega = 2/\Delta t$, where Δt is the pulse duration. Then we calculate the dipole moments $d_n(t)$ in real time using Eq. (1). We assume that the incident field illuminates the first particle in the chain only. Correspondingly, we set $E_n^{(\mathrm{inc})} = e\delta_{n1}$ in Eq. (2), where e is the vector of polarization. We then solve Eq. (2) numerically by direct matrix inversion for a set of discrete frequencies sampled with sufficiently high density and in a sufficiently wide interval. Finally, we obtain the real-time dipole moments $d_n(t)$ by evaluating the integral (1) numerically by the trapezoidal rule.

In what follows, we consider SPP propagation in chains of spheres and spheroids. We use the chain parameters that can be considered as "optimal" for a given particle shape. In the case of spheroids, we use $b = 8$ nm, $a = 20$ nm (this corresponds to $\xi = b/a = 0.4$), and $h = 24$ nm ($h/b = 3$). For comparison, we also show the results for spheres with $a = b = 8$ nm. The pulse duration is set to $\Delta t = 1$ fs. We chose the central frequencies of the pulses, ω_0, to be in the range of the real parts of the natural frequencies of a given chain with the mode indices $m_k > 2$. This choice ensures effective coupling of the incident electromagnetic energy to the waveguiding modes of the chain. We have used different central frequencies for different chains and different SPP polarizations, and the specific values of ω_0 are shown in the figure labels. We plot the dimensionless function

$$\mathcal{F}_n(t) = \left|\frac{d_n(t)}{d_1(0)}\right|. \tag{9}$$

The normalization factor in this formula is somewhat arbitrary, and it is only used to obtain a numerical result of the order of unity. Finally, time will be displayed in all plots in the units of

$$\tau = h/c. \tag{10}$$

In Fig. 7 we illustrate the time evolution of $\mathcal{F}_n(t)$ in a chain of spherical particles. As follows from the data of Fig. 3, wave packets in such chains propagate faster in the case of L polarization. From the physical point of view, smaller values of group velocity cause longer interaction of SPPs with metal

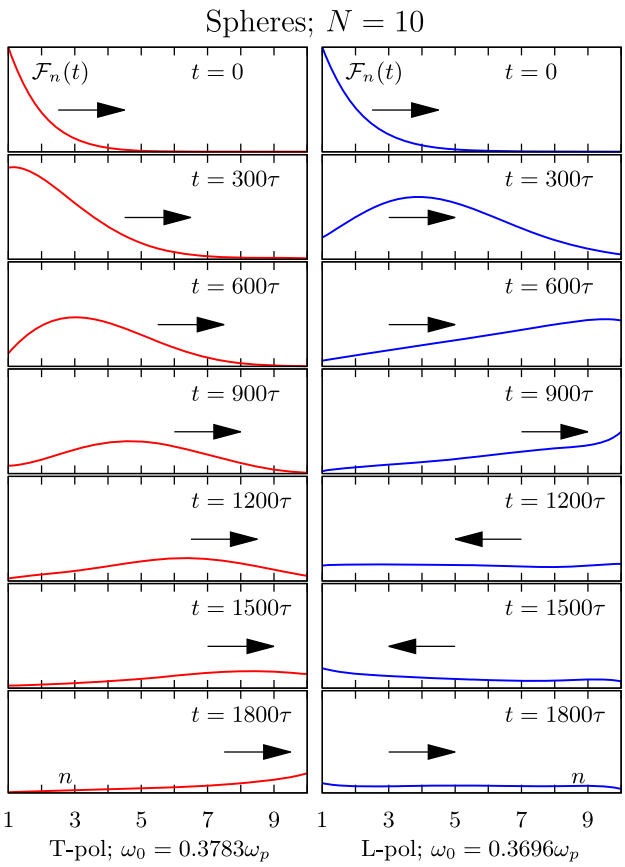

Fig. 7. Propagation of wave packets in a chain of $N = 10$ spherical particles with the radius $a = b = 8$ nm for the SPP polarizations and central pulse frequencies as labeled. The quantity $\mathcal{F}_n(t)$ is shown as a function of the index n that labels the particles at different instances of time t. Here and in subsequent figures, arrows indicate the direction of wave packet propagation. The same vertical scale from 0 to 1 is used in all subplots of this figure. The incident pulse duration is $\Delta t = 1$ fs.

and larger ohmic losses as a consequence. In agreement with this observation, we have $\mathcal{F}_{10}(1800\tau) \approx 0.2$ in the case of T polarization and $\mathcal{F}_{10}(900\tau) \approx 0.4$ in the case of L polarization.

The pattern of wave packet propagation changes substantially when we replace spheres with spheroids. Consider first the case of prolate spheroids, which is illustrated in Fig. 8. As was discussed above, the SPP group velocity in such chains is several times higher than in chains made of spherical particles. Indeed, the wave packets shown in Fig. 8 reach the end of the chain approximately six times faster for T polarization and two times faster for L polarization as compared to a chain of spherical particles with the same ratio h/b (Fig. 7). Correspondingly, SPP decay is not as pronounced in Fig. 8 as it is in Fig. 7.

The most favorable waveguide configuration in terms of propagation time and total attenuation is a chain of oblate spheroids. Electromagnetic interaction of particles in this case is the strongest when compared to all other chains with the same ratio of h/b. Correspondingly, the group velocities are largest and SPP decay is slowest. SPP propagation dynamics in chains of this type are illustrated in Fig. 9. It can be seen that the signal reaches the end of the chain in only $150\tau =$ 12 fs and almost without decay in the cases of both T and

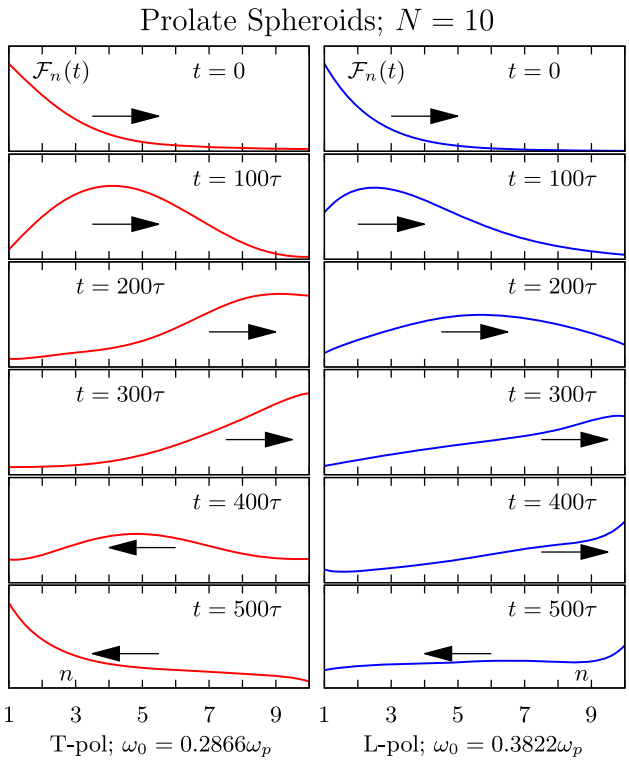

Fig. 8. Same as in Fig. 7 but for a chain of prolate spheroids with $a = 20$ nm, $b = 8$ nm ($\xi = b/a = 0.4$), and $h = 24$ nm. The same vertical scale from 0 to 1.2 is used in all subplots of this figure.

L polarization. However, multiple reflections from the chain terminals can clearly play a detrimental role in information processing.

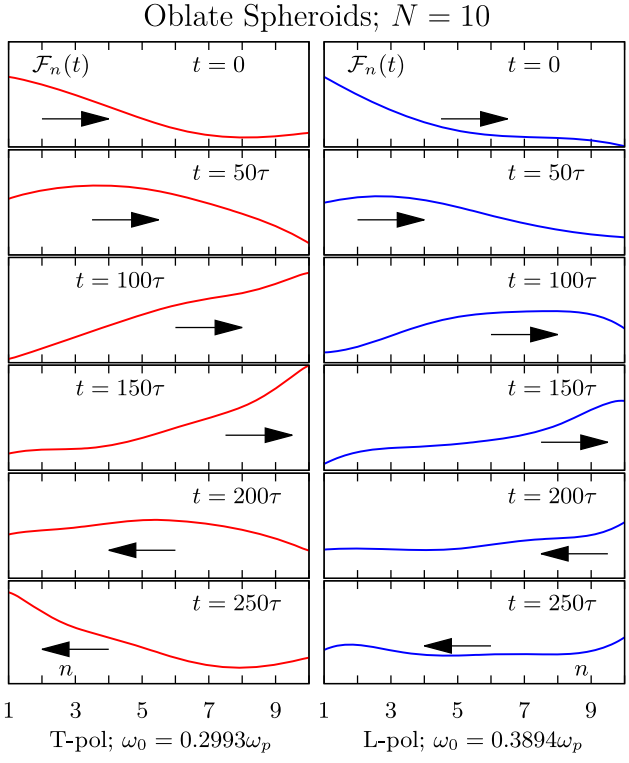

Fig. 9. Same as in Fig. 7 but for a chain of oblate spheroids with $a = 20$ nm, $b = 8$ nm ($\xi = b/a = 0.4$), and $h = 24$ nm. The same vertical scale from 0 to 1.5 is used in all subplots of this figure.

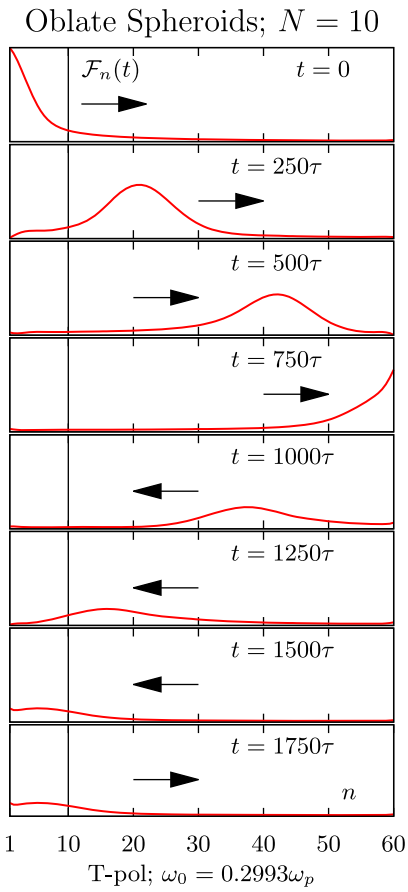

Fig. 10. Propagation of a wave packet in the same chain of oblate spheroids as in Fig. 9 but with $N = 60$ particles. It is assumed that the signal readout occurs at the site $n = 10$ (indicated by the vertical line). The rest of the chain is used as a dissipative trap whose function is to suppress parasitic effects of reflections.

To avoid the problem noted above, we propose to use somewhat longer chains but read out the signal at an intermediate site. The rest of the chain (the tail) functions in this case as a dissipative trap. In the simplest case that we consider here, the trap has the same parameters h, b, and a as the "working" segment of the chain. Violation of this condition can cause parasitic reflections at the junction. However, we note that other types of traps are also possible. What is important here is that the working segment of the chain and the trap are impedance-matched. Technologically, traps can be placed beyond the working layer of a chip to minimize interference with the working logical elements in the basic layer.

We illustrate the idea of an absorptive trap in Fig. 10, where we consider a chain of $N = 60$ oblate spheroids of the same type as were used to generate the data for Fig. 9. We assume, however, that the signal is read out at the $n = 10$ site. As a wave packet travels beyond this site to the far end of the chain, it experiences decay due to ohmic losses, and the amplitude of the first reflection that arrives at the readout site is already negligibly small.

6. SUMMARY

We have used the dipole approximation and the fully retarded electromagnetic interaction model to compute numerically the waveguiding modes and discrete dispersion relations of short ($N = 10$) plasmonic chains of silver nanoparticles of both spherical and spheroidal shape. We have also simulated the dynamics of femtosecond wave packet propagation in such chains. We have found that the most efficient transport of plasmonic excitations (that is, with minimum decay and maximum group velocity) occurs in chains of oblate spheroids with sufficiently small values of the aspect ratio b/a (e.g., $b/a = 0.4$). Further reduction of the aspect ratio allows one to further increase the group velocities but also affects large radiative losses in finite chains.

Reflection of wave packets from the terminals of short chains results in an overlap of the reflected and direct pulses. This parasitic effect is detrimental for information processing. We have shown, however, that the use of a simple dissipative trap, which is placed at the far end of the chain, can reduce the amplitude of the reflected signal by an order of magnitude or more. The dissipative trap must be impedance-matched to the working segment of the waveguide, and the simplest configuration in which such matching takes place is simply an additional segment of the same chain. If this approach is used, the signal is read out at an intermediate site of a chain. The chain tail beyond the readout site serves then as a dissipative trap. We have illustrated the reduction of parasitic effects at the readout site in numerical simulations (Fig. 2).

ACKNOWLEDGMENTS

This research was supported in part by the U.S. National Science Foundation under Grant DMS1216970; by the Russian Academy of Sciences under Grants 24.29, 24.31, III.9.5, 43, and SFU (101); and by the Russian Ministry of Education and Science under Contract 1792.

REFERENCES AND NOTES

1. A. Alu and N. Engheta, "Theory of linear chains of metamaterial/plasmonic particles as subdiffraction optical nanotrasmission lines," Phys. Rev. B **74**, 205436 (2006).
2. D. S. Citrin, "Plasmon-polariton transport in metal-nanoparticle chains embedded in a gain medium," Opt. Lett. **31**, 98–100 (2006).
3. K. B. Crozier, E. Togan, E. Simsek, and T. Yang, "Experimental measurement of the dispersion relations of the surface plasmon modes of metal nanoparticle chains," Opt. Express **15**, 17482–17493 (2007).
4. A. A. Govyadinov and V. A. Markel, "From slow to superluminal propagation: dispersive properties of surface plasmon polaritons in linear chains of metallic nanospheroids," Phys. Rev. B **78**, 035403 (2008).
5. M. Conforti and M. Guasoni, "Dispersive properties of linear chains of lossy metal nanoparticles," J. Opt. Soc. Am. B **27**, 1576–1582 (2010).
6. Y. Hadad and B. Z. Steinberg, "Green's function theory for infinite and semi-infinite particle chains," Phys. Rev. B **84**, 125402 (2011).
7. M. Guasoni and M. Conforti, "Complex dispersion relation of a double chain of lossy metal nanoparticles," J. Opt. Soc. Am. B **28**, 1019–1025 (2011).
8. T. Cheng, C. Rangan, and J. E. Sipe, "Metallic nanoparticles on waveguide structures: effects on waveguide mode properties and the promise of sensing applications," J. Opt. Soc. Am. B **30**, 743–765 (2013).
9. P. J. Compaijen, V. A. Malyshev, and J. Knoester, "Surface-mediated light transmission in metal nanoparticle chains," Phys. Rev. B **87**, 205437 (2013).
10. C. Lee, M. Tame, C. Noh, J. Lim, S. A. Maier, J. Lee, and D. J. Angelakis, "Robust-to-loss entanglement generation using a quantum plasmonic nanoparticle array," New J. Phys. **15**, 083017 (2013).

11. R. S. Savelev, A. P. Slobozhanyuk, A. E. Miroshnichenko, Y. S. Kivshar, and P. A. Belov, "Subwavelength waveguides composed of dielectric nanoparticles," Phys. Rev. B **89**, 035435 (2014).
12. D. E. Chang, A. S. Sorensen, P. R. Hemmer, and M. D. Lukin, "Strong coupling of single emitters to surface plasmons," Phys. Rev. B **76**, 035420 (2007).
13. A. H. Rose, B. M. Wirth, R. E. Hatem, A. P. Rashed Ahmed, J. Burns, M. J. Naughton, and K. Kempa, "Nanoscope based on nanowaveguides," Opt. Express **22**, 5228–5233 (2014).
14. X. Zhang, Z. Li, J. J. Chen, S. Yue, and Q. H. Gong, "A dichroic surface-plasmon-polariton splitter based on an asymmetric T-shape nanoslit," Opt. Express **21**, 14548–14554 (2013).
15. Z. Han and S. I. Bozhevolnyi, "Radiation guiding with surface plasmon polaritons," Rep. Prog. Phys. **76**, 016402 (2013).
16. M. L. Brongersma, J. W. Hartman, and H. A. Atwater, "Electromagnetic energy transfer and switching in nanoparticle chain arrays below the diffraction limit," Phys. Rev. B **62**, R16356 (2000).
17. S. Y. Park and D. Stroud, "Surface-plasmon dispersion relation in chains of metallic nanoparticles: an exact quasistatic calculation," Phys. Rev. B **69**, 125418 (2004).
18. W. H. Weber and G. W. Ford, "Propagation of optical excitations by dipolar interactions in metal nanoparticle chains," Phys. Rev. B **70**, 125429 (2004).
19. C. R. Simovski, A. J. Viitanen, and S. A. Tretyakov, "Resonator mode in chains of silver spheres and its possible application," Phys. Rev. E **72**, 066606 (2005).
20. A. F. Koenderink and A. Polman, "Complex response and polariton-like dispersion splitting in periodic metal nanoparticle chains," Phys. Rev. B **74**, 033402 (2006).
21. K. H. Fung and C. T. Chan, "Plasmonic modes in periodic metal nanoparticle chains: a direct dynamic eigenmode analysis," Opt. Lett. **32**, 973–975 (2007).
22. A. F. Koenderink, "Plasmon nanoparticle array waveguides for single photon and single plasmon sources," Nano Lett. **9**, 4228–4233 (2009).
23. I. B. Udagedara, I. D. Rukhlenko, and M. Premaratne, "Surface plasmon-polariton propagation in piecewise linear chains of composite nanospheres: the role of optical gain and chain layout," Opt. Express **19**, 19973–19986 (2011).
24. B. Rolly, N. Bonod, and B. Stout, "Dispersion relations in metal nanoparticle chains: necessity of the multipole approach," J. Opt. Soc. Am. B **29**, 1012–1019 (2012).
25. S. A. Maier, P. G. Kik, and H. A. Atwater, "Observation of coupled plasmon-polariton modes in Au nanoparticle chain waveguides of different length: estimation of waveguide loss," Appl. Phys. Lett. **81**, 1714–1716 (2002).
26. I. L. Rasskazov, V. A. Markel, and S. V. Karpov, "Transmission and spectral properties of short optical plasmon waveguides," Opt. Spectrosc. **115**, 666–674 (2013).
27. I. L. Rasskazov, S. V. Karpov, and V. A. Markel, "Surface plasmon polaritons in curved chains of metal nanoparticles," Phys. Rev. B **90**, 075405 (2014).
28. S. A. Maier, P. G. Kik, and H. A. Atwater, "Optical pulse propagation in metal nanoparticle chain waveguides," Phys. Rev. B **67**, 205402 (2003).
29. V. A. Markel and A. K. Sarychev, "Propagation of surface plasmons in ordered and disordered chains of metal nanospheres," Phys. Rev. B **75**, 085426 (2007).
30. B. Auguie and W. L. Barnes, "Diffractive coupling in gold nanoparticle arrays and the effect of disorder," Opt. Lett. **34**, 401–403 (2009).
31. D. Van Orden, Y. Fainman, and V. Lomakin, "Optical waves on nanoparticle chains coupled with surfaces," Opt. Lett. **34**, 422–424 (2009).
32. V. A. Markel, "Coupled-dipole approach to scattering of light from a one-dimensional periodic dipole chain," J. Mod. Opt. **40**, 2281–2291 (1993).
33. F. Claro and R. Fuchs, "Collective surface modes in a fractal cluster of spheres," Phys. Rev. B **44**, 4109–4116 (1991).
34. C. F. Bohren and D. R. Huffman, *Absorption and Scattering of Light by Small Particles* (Wiley, 1998).
35. I. B. Udagedara, I. D. Rukhlenko, and M. Premaratne, "Complex-ω approach versus complex-k approach in description of gain-assisted surface plasmon-polariton propagation along linear chains of metallic nanospheres," Phys. Rev. B **83**, 115451 (2011).
36. B. T. Draine, "The discrete-dipole approximation and its application to interstellar graphite grains," Astrophys. J. **333**, 848–872 (1988).
37. V. A. Markel, "Scattering of light from two interacting spherical particles," J. Mod. Opt. **39**, 853–861 (1992).
38. I. L. Rasskazov, S. V. Karpov, and V. A. Markel, "Nondecaying surface plasmon polaritons in linear chains of silver nanospheroids," Opt. Lett. **38**, 4743–4746 (2013).
39. We note that the concept of group velocity is only valid as long as $-\mathrm{Im}(\Omega)$ is sufficiently small.